Multiferroic quantum criticality

Author(s):
Narayan, Awadhesh; Cano, Andrés; Balatsky, Alexander V.; Spaldin, Nicola

Publication date:
2019-03

Permanent link:
https://doi.org/10.3929/ethz-b-000396679

Originally published in:
Nature Materials 18(3), https://doi.org/10.1038/s41563-018-0255-6

nature materials

ARTICLES

https://doi.org/10.1038/s41563-018-0255-6

Multiferroic quantum criticality

Awadhesh Narayan[1], Andrés Cano[1,2], Alexander V. Balatsky[3,4,5] and Nicola A. Spaldin[1*]

The zero-temperature limit of a continuous phase transition is marked by a quantum critical point, which can generate physical effects that extend to elevated temperatures. Magnetic quantum criticality is now well established, and has been explored in systems ranging from heavy fermion metals to quantum Ising materials. Ferroelectric quantum critical behaviour has also been recently demonstrated, motivating a flurry of research investigating its consequences. Here, we introduce the concept of multiferroic quantum criticality, in which both magnetic and ferroelectric quantum criticality occur in the same system. We develop the phenomenology of multiferroic quantum criticality and describe the associated experimental signatures, such as phase stability and modified scaling relations of observables. We propose several material systems that could be tuned to multiferroic quantum criticality utilizing alloying and strain as control parameters. We hope that these results stimulate exploration of the interplay between different kinds of quantum critical behaviours.

In conventional thermal phase transitions, ordered phases of matter transition to disordered phases with increasing temperature. Examples of these transitions include ferromagnet to paramagnet or conventional superconductor to normal metal. In a classical universe, zero-temperature fluctuation-driven phase transitions cannot occur because of the absence of thermal fluctuations. Quantum mechanics offers richer possibilities, because the quantum fluctuations that occur even at zero temperature can give rise to zero-temperature phase transitions on varying a non-thermal control parameter g, such as pressure or doping (Fig. 1a). The critical point in such a quantum phase transition is called a quantum critical point (QCP)[1].

Although the QCP that separates the ordered and disordered phases occurs by definition only at zero temperature, it strongly influences finite-temperature behaviour because of the interplay between quantum and thermal fluctuations. This yields a characteristic quantum critical 'fan' (Fig. 1b) that has been extensively studied in magnets. This is generically associated with unconventional features, such as non-classical scaling of correlation functions[2], appearance of emergent symmetries[3] and breakdown of the quasiparticle picture in metals[4]. In addition, quantum critical fluctuations provide a fertile ground for the emergence of interesting phases, including unconventional superconductivity, for example in heavy fermion metals close to their magnetic quantum critical point[5].

Materials in the vicinity of ferroelectric to paraelectric phase transitions are attracting renewed interest[6]. Quantum criticality theory applied to ferroelectrics[7,8] predicts measurable signatures in the dielectric constant, and the quantum paraelectrics $SrTiO_3$ and $KTaO_3$ indeed exhibit the expected scaling over a broad temperature range[6]. Based on these insights, ferroelectric quantum critical behaviour has been suggested as the origin of superconductivity in doped $SrTiO_3$, with critical fluctuations of the ferroelectric mode proposed as the 'glue' for Cooper pairs[9]. Specifically, it was shown theoretically[9], and confirmed experimentally in isotope- and Ca-substituted samples[10,11], that such a mechanism causes strong enhancement of the superconducting critical temperature as the system is pushed closer to the ferroelectric QCP.

Here we introduce the concept of multiferroic quantum criticality (MFQC), in which magnetic and ferroelectric QCPs occur in the same system. Multiferroic materials, with their coexisting polarization and magnetization, are of fundamental interest due to the coupling between these different orders[12] and provide an ideal platform for studying the coupling and competition between orders at low temperature. We identify a number of specific material systems within the family of established multiferroics in which MFQC should be realizable and describe the experimental signatures and properties associated with a multiferroic QCP.

Phenomenology of multiferroic quantum criticality

We consider a system described by an effective action of the form[13,14] $S=S_\phi+S_\psi+S_{\phi\psi}$, where

$$S_\phi=\int d^dr\,d\tau\left[-\alpha_\phi\,|\boldsymbol{\phi}|^2+\frac{1}{2}\beta_\phi\,|\boldsymbol{\phi}|^4+\frac{1}{2}\,|\partial_\mu\boldsymbol{\phi}|^2\right] \tag{1}$$

$$\begin{aligned}S_\psi &= \int d^dr\,d\tau\left[-\alpha_\psi\,|\boldsymbol{\psi}|^2+\frac{1}{2}\beta_\psi\,|\boldsymbol{\psi}|^4\right]\\ &+\int d^dk\,d\omega\left[\frac{k^2}{2}+\gamma\frac{\omega}{k^{z-2}}\right]|\boldsymbol{\psi}|^2\end{aligned} \tag{2}$$

Here $\boldsymbol{\phi}$ and $\boldsymbol{\psi}$ are real, multiple-component fields representing the ferroelectric and magnetic order parameters, and the index $\mu=0, 1, \ldots, d$ runs over time and d spatial dimensions. α and β are the coefficients of the quadratic and biquadratic terms of the effective action, r and τ denote position and imaginary time, k and ω the momentum and frequency, and we choose units such that the propagation speed for both fields is unity. The actions describe continuous ferroelectric and magnetic phase transitions with dynamical exponents equal to one for $\boldsymbol{\phi}$ and z for $\boldsymbol{\psi}$ (refs. [13,14]). For individual fields, the customary quartic interactions $S_\phi^{\rm int}=\frac{\beta_\phi}{2}\int d^dr\,d\tau\,|\boldsymbol{\phi}|^4$ and $S_\psi^{\rm int}=\frac{\beta_\psi}{2}\int d^dr\,d\tau\,|\boldsymbol{\psi}|^4$, give rise to susceptibilities, χ, scaling with temperature as $\chi_\phi^{-1}\sim T^{d-1}$ and $\chi_\psi^{-1}\sim T^{(d+z-2)/z}$ (for $d+z>4$; small logarithmic corrections are expected at low temperatures for $d+z=4$; ref. [15]). In three dimensions, this leads to dielectric susceptibility $\chi_\phi^{-1}\sim T^2$ for a quantum critical ferroelectric and magnetic susceptibility $\chi_\psi^{-1}\sim T^{3/2}$ for an antiferromagnet ($z=2$). Note that

[1]Materials Theory, ETH Zurich, Zurich, Switzerland. [2]Institut Néel, CNRS & Univ. Grenoble Alpes, Grenoble, France. [3]NORDITA, Stockholm, Sweden. [4]Institute for Materials Science, Los Alamos, NM, USA. [5]Department of Physics, University of Connecticut, Storrs, CT, USA. *e-mail: nicola.spaldin@mat.ethz.ch

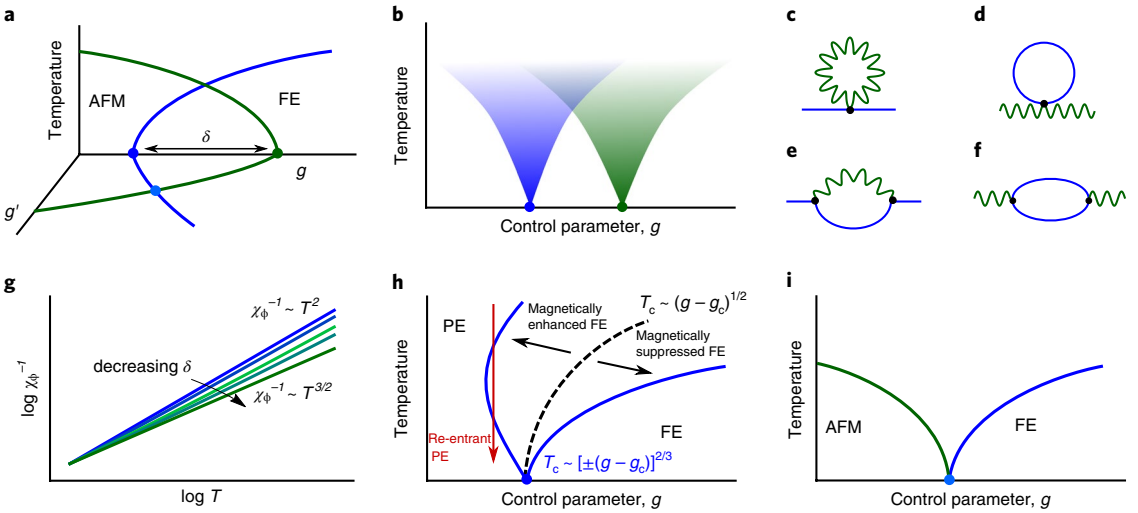

Fig. 1 | Phenomenology and identification of multiferroic quantum criticality. a, Antiferromagnetic (AFM) and ferroelectric (FE) quantum critical points generically occur at different values of a control parameter, g. The separation between the two critical points, δ, can be tuned by an additional control parameter, g', and can lead to a fine-tuned bicritical point. **b**, Schematic of quantum criticality regions arising from the zero-temperature (T) magnetic and ferroelectric critical points. Note the overlapping region in which magnetoelectric quantum critical excitations are expected. **c**–**f**, Feynman diagrams for one loop correction to the susceptibilities with biquadratic coupling (**c**,**d**) and dynamical coupling (**e**,**f**). The solid and wavy lines represent the propagators for ferroelectric and magnetic order parameters, respectively. **g**, Temperature scaling of inverse dielectric susceptibility, χ_ϕ^{-1}, for biquadratic coupling with decreasing separation between the quantum critical points, δ. A crossover from an exponent of 2 to 3/2 is predicted as δ decreases. **h**, Modification of the ferroelectric phase diagram due to the multiferroic quantum criticality that accompanies this crossover. The ferroelectric phase can be either enhanced or suppressed by the quantum critical magnetic degrees of freedom, which can lead to a re-entrant behaviour of the paraelectric (PE) phase as a function of the temperature (red arrow). In both cases, the critical exponents of the magnetic sector will take over the scaling of the ferroelectric critical temperature, T_c, with the control parameter. Here g_c is the critical value of the control parameter. **i**, A coupled bicritical point can occur when the two quantum critical points are coincident with variation of a single control parameter.

the dynamics arising from a ferromagnetic QCP ($z=3$) are different from those of an antiferromagnetic one ($z=2$).

When these two QCPs occur in the same system, the separation between them, δ, can be tuned by using an additional control parameter g' (Fig. 1a), and the interaction between the fields (Fig. 1c,d) leads to measurable signatures in the scaling of observables, as we show in the following.

First we review the effect of a biquadratic interaction

$$S^0_{\phi\psi} = \frac{g_0}{2}\int d^d r\,\mathrm{d}\tau\ |\boldsymbol{\phi}|^2|\boldsymbol{\psi}|^2 \tag{3}$$

which is allowed by symmetry for all pairs of fields. $S^0_{\phi\psi}$ produces additional contributions to the susceptibilities (Fig. 1c,d), such that the overall fluctuations at the bicritical point are governed by the phase with the lower exponent[14,16]. Therefore, χ_ϕ^{-1} shows a crossover from T^2 to $T^{3/2}$ scaling, as the antiferromagnetic QCP approaches the ferroelectric one (Fig. 1g). On the other hand, χ_ψ^{-1} continues to follow $T^{3/2}$ scaling, unaffected by the proximity of the ferroelectric QCP.

We note that such a biquadratic interaction can lead to qualitative changes in the phase diagram. Specifically, the sign of the aforementioned corrections to χ_ϕ^{-1} is determined by g_0 itself and therefore can be either positive or negative. Consequently, the proximity of the magnetic QCP can either suppress or enhance the ferroelectric phase and change the scaling of the corresponding critical temperature, T_c, as a function of the control parameter as illustrated in Fig. 1h. Interestingly, this can lead to a situation in which, by reducing the temperature, the paraelectric phase displays a re-entrant behaviour due to the MFQC (Fig. 1h).

In our MFQC case, $\boldsymbol{\phi}$ is associated with a polar distortion and $\boldsymbol{\psi}$ with magnetic order. Consequently, two additional interactions of lower order than the biquadratic are allowed by symmetry. First, a gradient interaction of the form

$$S^1_{\phi\psi} = g_1\int d^d r\,\mathrm{d}\tau\,\boldsymbol{\phi}\cdot[\boldsymbol{\psi}(\nabla\cdot\boldsymbol{\psi})-(\boldsymbol{\psi}\cdot\nabla)\boldsymbol{\psi}] \tag{4}$$

corresponding to the inverse Dzyaloshinskii–Moriya interaction responsible for the spin-induced polarization in spiral magnets[17,18]. Second, the dynamical counterpart of this interaction

$$S^2_{\phi\psi} = g_2\int d^d r\,\mathrm{d}\tau\,\boldsymbol{\psi}\cdot(\boldsymbol{\phi}\times\partial_\tau\boldsymbol{\phi}) \tag{5}$$

which can be spin–orbit coupling or exchange driven[19,20], becomes important in the vicinity of quantum phase transitions. Using finite-temperature field theory[21], we find that the $S^2_{\phi\psi}$ interaction gives a correction to χ_ϕ^{-1} proportional to

$$\begin{aligned} k_\mathrm{B}T\sum_n\int d^d k\frac{\omega_n^2}{\left(-\alpha_\phi+\frac{k^2}{2}+\frac{\omega_n^2}{2}\right)\left(-\alpha_\psi+\frac{k^2}{2}+\gamma\frac{\omega_n}{k^{z-2}}\right)} \\ = \int d^d k k^{z-2}\left[\frac{\omega_\phi}{2}\frac{\omega_\psi-\omega_\phi+2\omega_\psi n_\mathrm{B}(\omega_\phi)}{\omega_\phi^2-\omega_\psi^2}+\frac{\omega_\psi^2 n_\mathrm{B}(\omega_\psi)}{\omega_\psi^2-\omega_\phi^2}\right] \end{aligned} \tag{6}$$

where $\omega_n = 2\pi n k_\mathrm{B}T$ ($n=0,\pm1,\ldots$) are bosonic Matsubara frequencies, k_B is the Boltzmann constant, $\pm\omega_\phi = \pm\sqrt{-\alpha_\phi+k^2/2}$ and $\omega_\psi = \frac{1}{\gamma}(-\alpha_\psi k^{z-2}+k^z/2)$, with $n_\mathrm{B}(\omega)=\frac{1}{e^{\omega/k_\mathrm{B}T}-1}$ being the Bose function. The corresponding Feynman diagram is shown in Fig. 1e. Evaluating the integral over the momenta in three dimensions, we obtain

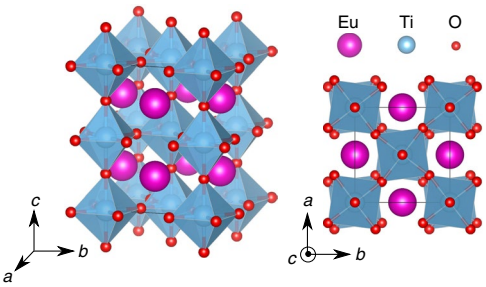

Fig. 2 | Crystal structure of $EuTiO_3$. Europium titanate forms in the perovskite structure with antiferrodistortive rotations around the c axis ($a^0a^0c^-$ in Glazer notation).

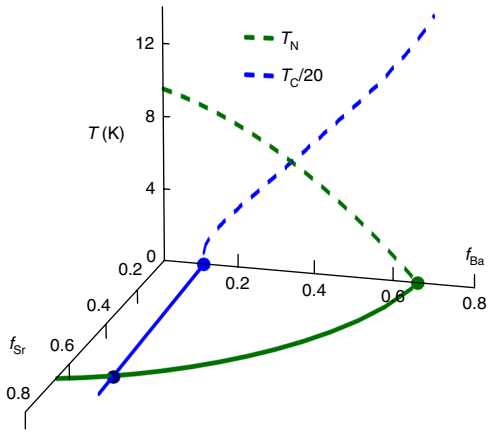

Fig. 3 | Tuning criticality in $EuTiO_3$ by alloying. Temperature–concentration phase diagram of (Eu,Ba,Sr)TiO_3. Dashed lines show the finite temperature phase boundaries of antiferromagnetic (green) and ferroelectric (blue) phases with increasing Ba concentration, f_{Ba}, with no Sr. Solid lines track magnetic (green) and ferroelectric (blue) quantum critical points with increasing Sr concentration, f_{Sr}. A fine-tuned bicritical point is reached at the crossing of the two, at a composition $Eu_{0.3}Ba_{0.1}Sr_{0.6}TiO_3$. Here T_N and T_c are the Néel temperature and ferroelectric critical temperature, respectively.

$$\chi_\phi^{-1} \sim T^{3-1/z} \tag{7}$$

to lowest order in temperature as the two QCPs come close together, remarkably different from the simplest biquadratic coupling case in which the field with the lower exponent dominates. Instead, for proximal ferroelectric and antiferromagnetic ($z=2$) QCPs, we find that these unconventional corrections yield $\chi_\phi^{-1} \sim T^{5/2}$ as a subdominant correction to the dielectric susceptibility arising from the influence of magnetic criticality, with the leading term scaling as T^2. A similar calculation for the magnetic susceptibility, by evaluating the diagram shown in Fig. 1f, yields $\chi_\psi^{-1} \sim T^2$. The spatial gradient term, $S^1_{\phi\psi}$, leads to higher-order corrections to these scaling expressions ($\chi_\phi^{-1} \sim T^{2z}$).

We expect that this interplay between QCPs will lead to similar crossovers in other quantum critical scaling laws. For example, the Grüneisen parameter Γ, which is the ratio of the thermal expansion coefficient to the specific heat[22], diverges as $\Gamma \sim T^{-1/\nu z}$ in the quantum critical regime. Therefore, multiferroic quantum critical behaviour should manifest as different scaling of Γ near antiferromagnetic ($\Gamma \sim T^{-1}$) and ferroelectric ($\Gamma \sim T^{-2}$) QCPs. Note that the exponents of Γ obtained from scaling theory or mean field theory are similar at the upper critical dimension[15].

Finally, a special case of 'coupled bicriticality' occurs when variation of a single control parameter results in coincident magnetic and ferroelectric QCPs, as shown in Fig. 1i. To evaluate the behaviour in this regime, we use the biquadratic coupled action as the starting point for a renormalization group analysis treating quantum fluctuations in both fields. Employing an ϵ-expansion and retaining terms to one loop order we obtain the set of flow equations for α_ϕ, α_ψ, β_ϕ, β_ψ and g_0 (ref. [13]). From an analysis of the flow trajectories, we find that the bicritical point is stable for $g_0 < \sqrt{\beta_\phi \beta_\psi}$, whereas larger g_0 gives runaway flow trajectories, indicative of first-order phase transitions.

Material candidates

Next, we propose material candidates for achieving MFQC. Europium titanate, $EuTiO_3$, crystallizes in the perovskite structure (Fig. 2) with antiferrodistortive rotations of the oxygen octahedra leading to a tetragonal $I4/mcm$ space group[23,24]. The localized $4f^7$ moments on the Eu^{2+} ions order in a G-type antiferromagnetic arrangement (with all nearest-neighbour spins oppositely aligned) at the low Néel temperature of 5.3 K because of their small interionic exchange interactions[25]. At the same time, $EuTiO_3$ has a large and diverging dielectric constant at low temperatures, indicative of its proximity to a ferroelectric phase transition[26]; this behaviour is strikingly similar to that of $SrTiO_3$. Recently, Das studied the temperature and magnetic-field dependence of the dielectric susceptibility in $EuTiO_3$ (ref. [27]). Here we extend this work to explore $EuTiO_3$ as a model system for MFQC, and describe two strategies, alloying and strain engineering, to engineer multiferroic QCPs.

$EuTiO_3$ can be readily alloyed with the canonical ferroelectric $BaTiO_3$ (ref. [28]), which suppresses the magnetic ordering through dilution, at the same time promoting ferroelectricity by increasing the volume and favouring off-centering of ions from their high-symmetry positions[28]. Alloying with the quantum paraelectric $SrTiO_3$ (ref. [29]), on the other hand, should reduce the Néel temperature without affecting the ferroelectric properties, because $EuTiO_3$ and $SrTiO_3$ have the same lattice constant. This flexibility allows for a rich multiferroic phase diagram, including control of the position of and separation between the magnetic and ferroelectric QCPs.

To analyse the phase diagram of the (Eu,Ba,Sr)TiO_3 system, we performed Ising and Heisenberg model simulations with parameters extracted from density functional calculations in this work or measurements reported in the literature (see Methods for details). The resulting phase diagram is shown in Fig. 3. First, we examine the effect of Ba concentration, f_{Ba}. The Néel temperature, T_N, is suppressed to zero giving a magnetic QCP at $f_{Ba} \approx 0.65$, close to the percolation limit on a cubic lattice. Ferroelectricity emerges from a ferroelectric QCP at $f_{Ba} \approx 0.1$. For intermediate compositions ($0.1 < f_{Ba} < 0.65$) a multiferroic phase is obtained. Next, we track the positions of the magnetic and ferroelectric QCPs with increasing Sr concentration, f_{Sr}, as Sr is substituted for Eu. The ferroelectric QCP remains unchanged with increasing f_{Sr}. On the other hand, the magnetic QCP moves to lower values of f_{Ba} as f_{Sr} is increased. Alloying with Sr therefore tunes the separation between the two QCPs. Interestingly, at $f_{Ba} \approx 0.1$ and $f_{Sr} \approx 0.6$—that is, for composition $Eu_{0.3}Ba_{0.1}Sr_{0.6}TiO_3$—a fine-tuned bicritical point, at which the magnetic and ferroelectric QCPs are coincident, occurs.

As a second possible tuning parameter, we explore strain, which has proved to be a useful tool to tune the properties of perovskite oxide thin films[30]. Indeed, under biaxial tensile strain imposed via coherent heteroepitaxy, $EuTiO_3$ has been reported to become a ferromagnetic ferroelectric[31,32]. We performed density functional calculations (see Methods for details) to explore the effect of biaxial strain on the quantum critical behaviour of $EuTiO_3$ using the low-temperature tetragonal $I4/mcm$ structure[23,24], in contrast to previous work, which assumed a cubic structure. We found that G-type

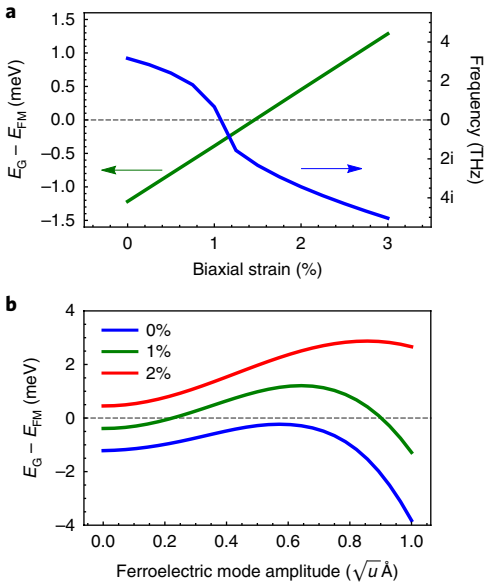

Fig. 4 | Near-bicriticality in strained $EuTiO_3$. a, Difference in energy, *E*, between G-type antiferromagnetic and ferromagnetic (FM) orders as a function of biaxial strain (green curve), from density functional calculations. Energy differences are in meV per *I4/mcm* unit cell. G-type order is favoured for less than ~1.4% strain, and ferromagnetic order at larger values. The blue curve shows the ferroelectric phonon mode frequency with G-type ordering as a function of strain. Imaginary (i) frequencies correspond to unstable phonon modes, indicative of a transition to a ferroelectric state. **b**, Energy difference between G-type and FM orders with increasing amplitude of the ferroelectric mode at different values of strain. Here, *u* is the atomic mass unit. At ~1% strain, close to the critical value, the system is both magnetically and structurally 'soft' and the relative stability of the magnetic orders can be reversed by varying the amplitude of the ferroelectric mode.

antiferromagnetic order is favoured for unstrained and small values of tensile biaxial strain, and ferromagnetic order becomes stable beyond ~1.4% strain (Fig. 4a). Although, the energy differences between different magnetic orders are small, we expect the general trends to be accurately described by density functional calculations. At a similar, though (in contrast to previous calculations[31]) not identical, value of critical strain, the ferroelectric phonon mode frequency becomes imaginary, indicating a ferroelectric instability. While biaxially strained $EuTiO_3$ is not precisely bicritical, the onset of ferroelectricity promotes ferromagnetic order, and our renormalization group analysis indicates that a first-order quantum phase transition will occur. The strong influence of the fluctuations in one order parameter on the other in this nearly bicritical scenario is strikingly revealed in Fig. 4b, where we plot the energy difference between the G-type antiferromagnetic and ferromagnetic orders with increasing ferroelectric mode amplitude. The magnetic energy difference is very sensitive to the amplitude of the ferroelectric mode, especially close to the critical strain, where the relative stability of G-type antiferromagnetic and ferromagnetic order is reversed with increasing ferroelectric mode amplitude.

In Table 1 we suggest other candidate materials for exploring multiferroic quantum criticality. Mn doping at the Sr or K sites in quantum paraelectric $SrTiO_3$ and $KTaO_3$ has been reported to result in a 'magnetoelectric multiglass' state with simultaneous polar and magnetic glassy states[33]. With appropriate choice of doping, these systems could be tuned to MFQC. Going beyond oxides, perovskite fluoride $NaMnF_3$ has been recently found to show quantum paraelectricity coexisting with G-type antiferromagnetic order[34].

Table 1 | Candidate materials for multiferroic quantum criticality

Material	Dielectric nature	Magnetic nature	Tuning strategy
$EuTiO_3$	Quantum paraelectric	G-type AFM ($T_N = 5.3$ K)[25]	Ba/Sr alloying at Eu site; strain
$SrTiO_3$	Quantum paraelectric	Diamagnetic[33]	Mn doping at Sr site
$KTaO_3$	Quantum paraelectric	Diamagnetic[33]	Mn doping at K site
$NaMnF_3$	Quantum paraelectric	G-type AFM ($T_N = 66$ K)[34]	Mg/Zn alloying at Mn site
$TbMnO_3$	Improper ferroelectric	spiral order ($T_N = 28$ K)[35]	Y/Eu alloying at Tb site

Suppressing the Néel temperature by Mg or Zn alloying at the Mn site could tune the magnetic sublattice to quantum criticality. Improper ferroelectrics, in which polarization arises as a secondary effect of a magnetic (or other lattice) ordering, are a promising class of materials to search for quantum bicritical multiferroics[35]. For example, in the canonical improper ferroelectric $TbMnO_3$, increasing the size of the rare earth ion by alloying with Eu changes the magnetic ground state from a spiral order to a collinear one, which drives a simultaneous quantum phase transition from a ferroelectric to a paraelectric state[36,37]. The dynamical coupling term, $S^2_{\phi\psi}$, is likely to dominate in this case, leading to our predicted unconventional scaling laws.

A promising route to engineer multiferroics has been through heterostructures and nanostructures[38]; such atomic-scale engineering could be used to create quantum critical multiferroics. For instance, the Néel temperature of $EuTiO_3/SrTiO_3$ superlattices could be tuned with the relative number of layers of the two components and reach criticality. Heterostructures of materials with magnetic QCPs (such as heavy fermions) and materials with ferroelectric QCPs (for example, $SrTiO_3$) could be used to achieve controllable and tunable composite or interfacial MFQC. With reduced spatial dimensions such systems could prove to be interesting playgrounds for exploring scaling laws below the upper critical dimension, distinct from bulk materials.

Implications and prospects

The effects of the coupled magnetoelectric critical excitations proposed here should manifest in an experimentally accessible temperature range. The temperature scales for observing universal quantum critical properties are related to the Néel temperature (~5 K in the case of $EuTiO_3$) for the magnetic part and the Debye temperature for the ferroelectric case. For the closely related quantum paraelectrics, $SrTiO_3$ and $KTaO_3$, the experimentally reported limit is ~50 K (ref. [6]).

Adding charge carriers would provide an additional non-thermal control parameter. From our preliminary calculations we find, for example, that doping of 5×10^{19} electrons cm^{-3} moves 1% biaxially strained $EuTiO_3$ to a magnetic QCP while hardening the ferroelectric phonon mode due to enhanced electrostatic screening between the electric dipoles. Similar trends of stabilization of ferromagnetic order and suppression of ferroelectricity with electron doping are also found in alloyed $EuTiO_3$. The presence of carriers could also lead to emergent modulated order within which QCPs are hidden, as has been observed recently in $NbFe_2$ (ref. [39]). Additionally, carriers offer the intriguing possibility of Fermi surface instabilities emerging around the critical points, potentially

enabling superconductivity. Close to an antiferromagnetic QCP, *d*-wave superconductivity is expected on a cubic lattice[40,41]. In contrast, a ferroelectric QCP would give rise to *s*-wave pairing[9]. Such an interplay between different kinds of pairing, arising from distinct QCPs, is an interesting avenue for future exploration.

Since ferroelectric and magnetic phase transitions can be discontinuous, it is important to determine the nature of the phase transitions in alloyed and strained $EuTiO_3$ and our other proposed systems. For example, perovskite $SrTiO_3$ and $KTaO_3$ show continuous phase transitions and the resulting quantum criticality[6], whereas a critical end point was recently observed at a magnetic-field-induced metaelectric phase transition in multiferroic $BiMn_2O_5$ (ref. [42]). While weakly first-order quantum phase transitions still lead to nearly critical fluctuations driving quantum criticality and could allow for observation of our proposals, first-order multiferroic quantum phase transitions could additionally be interesting in their own right. In this context, a recently proposed mechanism of 'quantum annealed criticality'[43], in which first-order finite-temperature phase transitions can end in a zero temperature critical point, could perhaps also be explored in our multiferroic quantum critical scenario. Discontinuous magnetic quantum phase transitions often result in intriguing phases such as magnetic rotons, instantons and skyrmion textures[44], and the implications associated with an additional breaking of space-inversion symmetry remain to be explored.

Criticality with multiple order parameters can also be engineered in ultracold quantum gases. A recent development in this direction is the demonstration of coupling and competition between two order parameters in a Bose–Einstein condensate coupled to two optical cavities[45]. We envisage that our predicted critical scaling crossovers arising from coupled order parameters of different types could also be explored in next-generation quantum gas–optical cavity systems.

In summary, we have introduced the concept of multiferroic quantum criticality, which combines magnetic and ferroelectric quantum critical behaviour in the same system. We have described the phenomenology of multiferroic quantum criticality, discussed its implications and presented suitable systems and schemes to realize it. Our work is particularly timely given the recent surge of interest in quantum materials[46], and we hope that our findings motivate the exploration of coupling and competition between various quantum critical behaviours.

Online content

Any methods, additional references, Nature Research reporting summaries, source data, statements of data availability and associated accession codes are available at https://doi.org/10.1038/s41563-018-0255-6.

Received: 25 November 2017; Accepted: 20 November 2018;
Published online: 31 December 2018

References

1. Sachdev, S. *Quantum Phase Transitions* 2nd edn (Cambridge Univ. Press, Cambridge, 2011).
2. Lake, B., Tennant, D. A., Frost, C. D. & Nagler, S. E. Quantum criticality and universal scaling of a quantum antiferromagnet. *Nat. Mater.* **4**, 329–334 (2005).
3. Coldea, R. et al. Quantum criticality in an Ising chain: experimental evidence for emergent E8 symmetry. *Science* **327**, 177–180 (2010).
4. Custers, J. et al. The break-up of heavy electrons at a quantum critical point. *Nature* **424**, 524–527 (2003).
5. Gegenwart, P., Si, Q. & Steglich, F. Quantum criticality in heavy-fermion metals. *Nat. Phys.* **4**, 186–197 (2008).
6. Rowley, S. E. et al. Ferroelectric quantum criticality. *Nat. Phys.* **10**, 367–372 (2014).
7. Khmelnitskii, D. E. & Shneerson, V. L. Low temperature displacement-type phase transition in crystals. *Sov. Phys. Solid State* **13**, 687 (1971).
8. Roussev, R. & Millis, A. J. Theory of the quantum paraelectric–ferroelectric transition. *Phys. Rev. B* **67**, 014105 (2003).
9. Edge, J. M., Kedem, Y., Aschauer, U., Spaldin, N. A. & Balatsky, A. V. Quantum critical origin of the superconducting dome in $SrTiO_3$. *Phys. Rev. Lett.* **115**, 247002 (2015).
10. Stucky, A. et al. Isotope effect in superconducting n-doped $SrTiO_3$. *Sci. Rep.* **6**, 37582 (2016).
11. Rischau, C. W. et al. A ferroelectric quantum phase transition inside the superconducting dome of $Sr_{1-x}Ca_xTiO_{3-\delta}$. *Nat. Phys.* **13**, 643–648 (2017).
12. Spaldin, N. A. & Fiebig, M. The renaissance of magnetoelectric multiferroics. *Science* **309**, 391–392 (2005).
13. She, J.-H., Zaanen, J., Bishop, A. R. & Balatsky, A. V. Stability of quantum critical points in the presence of competing orders. *Phys. Rev. B* **82**, 165128 (2010).
14. Morice, C., Chandra, P., Rowley, S. E., Lonzarich, G. & Saxena, S. S. Hidden fluctuations close to a quantum bicritical point. *Phys. Rev. B* **96**, 245104 (2017).
15. Chandra, P., Lonzarich, G. G., Rowley, S. E. & Scott, J. F. Prospects and applications near ferroelectric quantum phase transitions: a key issues review. *Rep. Progr. Phys.* **80**, 112502 (2017).
16. Oliver, G. T. & Schofield, A. J. Quantum multicriticality. Preprint at https://arxiv.org/abs/1506.03021 (2015).
17. Katsura, H., Nagaosa, N. & Balatsky, A. V. Spin current and magnetoelectric effect in noncollinear magnets. *Phys. Rev. Lett.* **95**, 057205 (2005).
18. Cheong, S.-W. & Mostovoy, M. Multiferroics: a magnetic twist for ferroelectricity. *Nat. Mater.* **6**, 13–20 (2007).
19. Dzyaloshinskii, I. E. & Mills, D. L. Intrinsic paramagnetism of ferroelectrics. *Philos. Mag.* **89**, 2079–2082 (2009).
20. Juraschek, D. M., Fechner, M., Balatsky, A. V. & Spaldin, N. A. Dynamical multiferroicity. *Phys. Rev. Mat.* **1**, 014401 (2017).
21. Abrikosov, A. A., Gorkov, L. P. & Dzyaloshinski, I. E. *Methods of Quantum Field Theory in Statistical Physics* (Dover, Mineola, 1975).
22. Zhu, L., Garst, M., Rosch, A. & Si, Q. Universally diverging Grüneisen parameter and the magnetocaloric effect close to quantum critical points. *Phys. Rev. Lett.* **91**, 066404 (2003).
23. Rushchanskii, K. Z., Spaldin, N. A. & Ležaić, M. First principles prediction of oxygen octahedral rotations in perovskite-structure $EuTiO_3$. *Phys. Rev. B* **85**, 104109 (2012).
24. Goian, V. et al. Antiferrodistortive phase transition in $EuTiO_3$. *Phys. Rev. B* **86**, 054112 (2012).
25. McGuire, T. R., Shafer, M. W., Joenk, R. J., Alperin, H. A. & Pickart, S. J. Magnetic structure of $EuTiO_3$. *J. Appl. Phys.* **37**, 981–982 (1966).
26. Kamba, S. et al. Magnetodielectric effect and optic soft mode behavior in quantum paraelectric $EuTiO_3$ ceramics. *EPL* **80**, 27002 (2007).
27. Das, N. Quantum critical behavior of a magnetic quantum paraelectric. *Phys. Lett. A* **376**, 2683–2687 (2012).
28. Rushchanskii, K. Z. et al. A multiferroic material to search for the permanent electric dipole moment of the electron. *Nat. Mater.* **9**, 649–654 (2010).
29. Guguchia, Z., Shengelaya, A., Keller, H., Köhler, J. & Bussmann-Holder, A. Tuning the structural instability of $SrTiO_3$ by Eu doping: the phase diagram of $Sr_{1-x}Eu_xTiO_3$. *Phys. Rev. B* **85**, 134113 (2012).
30. Schlom, D. G. et al. Strain tuning of ferroelectric thin films. *Annu. Rev. Mater. Res.* **37**, 589–626 (2007).
31. Fennie, C. J. & Rabe, K. M. Magnetic and electric phase control in epitaxial $EuTiO_3$ from first principles. *Phys. Rev. Lett.* **97**, 267602 (2006).
32. Lee, J. H. et al. A strong ferroelectric ferromagnet created by means of spin-lattice coupling. *Nature* **466**, 954–958 (2010).
33. Kleemann, W. et al. Multiglass order and magnetoelectricity in Mn^{2+} doped incipient ferroelectrics. *Eur. Phys. J. B* **71**, 407 (2009).
34. Dubrovin, R. M., Kizhaev, S. A., Syrnikov, P. P., Gesland, J.-Y. & Pisarev, R. V. Unveiling hidden structural instabilities and magnetodielectric effect in manganese uoroperovskites $AMnF_3$. *Phys. Rev. B* **98**, 060403 (2018).
35. Kimura, T. et al. Magnetic control of ferroelectric polarization. *Nature* **426**, 55–58 (2003).
36. Ishiwata, S. et al. Perovskite manganites hosting versatile multiferroic phases with symmetric and antisymmetric exchange strictions. *Phys. Rev. B* **81**, 100411 (2010).
37. Fedorova, N. S. et al. Relationship between crystal structure and multiferroic orders in orthorhombic perovskite manganites. *Phys. Rev. Mat.* **2**, 104414 (2018).
38. Ramesh, R. & Spaldin, N. A. Multiferroics: progress and prospects in thin films. *Nat. Mater.* **6**, 21–29 (2007).
39. Friedemann, S. et al. Quantum tricritical points in $NbFe_2$. *Nat. Phys.* **14**, 62–67 (2018).
40. Miyake, K., Schmitt-Rink, S. & Varma, C. M. Spin-fluctuation-mediated even-parity pairing in heavyfermion superconductors. *Phys. Rev. B* **34**, 6554 (1986).
41. Scalapino, D. J., Loh, E. Jr. & Hirsch, J. E. D-wave pairing near a spin-density-wave instability. *Phys. Rev. B* **34**, 8190 (1986).
42. Kim, J. W. et al. Observation of a multiferroic critical end point. *Proc. Natl Acad. Sci. USA* **106**, 15573–15576 (2009).
43. Chandra, P., Coleman, P., Continentino, M. A. & Lonzarich, G. G. Quantum annealed criticality. Preprint at https://arxiv.org/abs/1805.11771 (2018).

44. Peiderer, C. Why first order quantum phase transitions are interesting. *J. Phys. Condens. Matter* **17**, S987 (2005).
45. Morales, A., Zupancic, P., Léonard, J., Esslinger, T. & Donner, T. Coupling two order parameters in a quantum gas. *Nat. Mater.* **17**, 686–690 (2018).
46. Basov, D. N., Averitt, R. D. & Hsieh, D. Towards properties on demand in quantum materials. *Nat. Mater.* **16**, 1077–1088 (2017).

Acknowledgements

The authors acknowledge helpful discussions with G. Aeppli, T. Donner, K. Dunnett, C. Ederer, A. Edström, T. Esslinger, N. Fedorova, C. Gattinoni, Q. Meier, A. Morales, R. Pisarev and P. Zupancic. This work is supported by ETH-Zurich (A.N., A.C. and N.A.S.), the US DOE BES E3B7, the Villum Foundation and the Knut and Alice Wallenberg Foundation (A.V.B.). Calculations were performed at the Swiss National Supercomputing Centre (project ID p504).

Author contributions

N.A.S. conceived the concept. N.A.S., A.V.B., A.C. and A.N. devised the analysis. A.N. carried out the calculations. A.N. and N.A.S. wrote the manuscript with contributions from all authors.

Competing interests

The authors declare no competing interests.

Additional information

Reprints and permissions information is available at www.nature.com/reprints.

Correspondence and requests for materials should be addressed to N.A.S.

Publisher's note: Springer Nature remains neutral with regard to jurisdictional claims in published maps and institutional affiliations.

Methods

Finite-temperature field theory calculations. We write the free propagators for the two fields as

$$G_\phi = \frac{1}{-\alpha_\phi + k^2/2 + \omega^2/2} \tag{8}$$

$$G_\psi = \frac{1}{-\alpha_\psi + k^2/2 + \gamma\omega/k^{z-2}} \tag{9}$$

The $S^2_{\phi\psi}$ interaction gives a correction to χ_ϕ^{-1} of the form

$$\begin{aligned} & k_B T \sum_n \int d^d k G_\phi \omega_n^2 G_\psi \\ = & k_B T \sum_n \int d^d k \frac{\omega_n^2}{\left(-\alpha_\phi + \frac{k^2}{2} + \frac{\omega_n^2}{2}\right)\left(-\alpha_\psi + \frac{k^2}{2} + \gamma\frac{\omega_n}{k^{z-2}}\right)} \end{aligned} \tag{10}$$

We carry out the summation over the Matsubara frequencies using the standard contour integral technique[21], yielding

$$\int d^d k k^{z-2} \left[\frac{\omega_\phi(\omega_\psi - \omega_\phi)}{2(\omega_\phi^2 - \omega_\psi^2)} + \frac{\omega_\phi \omega_\psi n_B(\omega_\phi)}{\omega_\phi^2 - \omega_\psi^2} + \frac{\omega_\psi^2 n_B(\omega_\psi)}{\omega_\psi^2 - \omega_\phi^2} \right] \tag{11}$$

Close to criticality ($\alpha_\phi, \alpha_\psi \to 0$) in three dimensions, the third term gives the lowest exponent in the temperature dependence of $T^{3-1/z}$. This leads to the strongest correction to χ_ϕ^{-1}, as presented in equation (7) of the main text.

Density functional calculations. Our first-principles calculations were carried out using the Vienna ab-initio simulation package (VASP)[47] with the Perdew–Burke–Ernzerhof approximation to the exchange correlation functional[48]. Eu 4*f* electrons were treated with the GGA + *U* method, using Dudarev's approach[49], with $U = 6.0$ eV and $J = 1.0$ eV. Default projector augmented wave pseudopotentials were employed. A plane wave cutoff of 500 eV was used and the Brillouin zone was sampled using an $8\times8\times6$ *k*-point grid. Phonon calculations were performed using the phonopy code[50], with 80 atom supercells using a $4\times4\times6$ *k*-point mesh. For the biaxially strained $EuTiO_3$, the strain tensor reads

$$\varepsilon = \begin{pmatrix} \zeta & 0 & 0 \\ 0 & \zeta & 0 \\ 0 & 0 & -\nu\zeta \end{pmatrix} \tag{12}$$

where $\zeta = (a - a_0)/a_0$ is the applied strain (a_0 and a are the equilibrium and strained in-plane lattice constants) and ν is the biaxial Poisson ratio.

Ising model for estimating ferroelectric critical temperature. Ferroelectric alloys were modelled by a simple transverse Ising model[51], which has been shown to give reasonable estimates for experimental critical temperatures[52]:

$$\begin{aligned} H = & -\Omega \sum_i \sigma_i^x - \frac{1}{2}\sum_{ij} J_{ij}\sigma_i^z\sigma_j^z \\ & -\frac{1}{4}\sum_{ijkl} J_{ijkl}\sigma_i^z\sigma_j^z\sigma_k^z\sigma_l^z - 2\mu E\sum_i \sigma_i^z \end{aligned} \tag{13}$$

Here Ω is the tunnelling frequency and μ is the effective dipole moment, which couples to the external electric field E. $\sigma_i^{x,y,z}$ are pseudospins at the ith site, which interact via two-body (J_{ij}) and four-body (J_{ijkl}) exchange terms. The term proportional to σ_x is the tunnelling between the two minima of the free energy double well, and does not imply that the electric dipole has any precessional dynamics. Alloying is simulated by weighting the parameters by concentration of the constituents f_α:

$$J = \sum_\alpha f_\alpha J_\alpha, \quad \Omega = \sum_\alpha f_\alpha \Omega_\alpha, \quad \mu = \sum_\alpha f_\alpha \mu_\alpha \tag{14}$$

The polarization is then given by $P = 2n\mu\sum_i \langle\sigma_i^z\rangle$, where n is the number of dipoles per unit volume. The change of lattice parameter, a, with alloying is approximated using Vegard's law. Treating the pseudospin in the mean field approximation yields a self-consistent equation for the polarization, which is then solved numerically. The susceptibility $\chi = (\partial\langle P\rangle/\partial E)_{E=0}$ was used to estimate the critical temperatures for different alloy compositions. For $BaTiO_3$, the following model parameters were chosen: $J_{ij} = 23.90$ meV, $J_{ijkl} = 62.16$ meV, $\Omega = 30.58$ meV, $\mu = 2.17$ eÅ and $a = 4.005$ Å. For $SrTiO_3$ and $EuTiO_3$, the following parameters were selected: $J_{ij} = 2.04$ meV, $J_{ijkl} = 0$ meV, $\Omega = 6.86$ meV, $\mu = 1.51$ eÅ and $a = 3.905$ Å. The parameters used were previously fitted to reproduce the experimental values of critical temperatures and give good estimates of the experimental critical temperatures[52].

Heisenberg model for estimating magnetic critical temperature. The energies obtained from density functional calculations were mapped to a classical Heisenberg model to calculate the exchange parameters. The $4f^7$ moments on the Eu^{2+} are well localized, so the system can be reasonably described by a simple Heisenberg model. Alloying of non-magnetic ions (Sr and Ba) was modelled by introducing random binary variables ζ_i for each site i, such that

$$\begin{aligned} \zeta_i &= 1 \quad i = \text{Eu} \\ &= 0 \quad i = \text{Sr, Ba} \end{aligned} \tag{15}$$

This yields the Hamiltonian

$$H = -\sum_{ij} \mathcal{J}_{ij}\zeta_i\zeta_j S_i \cdot S_j + \sum_i \mathcal{D}_i\zeta_i S_i^2 \tag{16}$$

where S_i are classical spins at site i, $\mathcal{J}_{ij}$ is the nearest-neighbour exchange interaction strength and $\mathcal{D}_i$ is the single ion anisotropy energy. A competition between the exchange term, anisotropy term and dilution through alloying leads to a phase transition by tuning the α_ψ coefficient in the action (equation (2)). From density functional calculations, exchange interaction strengths were obtained to be $\mathcal{J}^{ab} = -0.0286$ meV (a–b plane exchange parameter) and $\mathcal{J}^c = 0.0331$ meV (c direction exchange parameter). The magnetic phases and critical temperatures of the system were then estimated using a standard Metropolis-based Monte Carlo procedure[53]. This simple treatment of disorder has previously been successfully applied to dilute magnetic semiconductors[54].

Data availability

The data that support the findings of this study are available from the corresponding author upon reasonable request.

References

47. Kresse, G. & Furthmüller, J. Efficient iterative schemes for ab initio total-energy calculations using a plane-wave basis set. *Phys. Rev. B* **54**, 11169 (1996).
48. Perdew, J. P., Burke, K. & Ernzerhof, M. Generalized gradient approximation made simple. *Phys. Rev. Lett.* **77**, 3865 (1996).
49. Dudarev, S. L., Botton, G. A., Savrasov, S. Y., Humphreys, C. J. & Sutton, A. P. Electron-energy-loss spectra and the structural stability of nickel oxide: an LSDA + U study. *Phys. Rev. B* **57**, 1505 (1998).
50. Togo, A. & Tanaka, I. First principles phonon calculations in materials science. *Scr. Mater.* **108**, 1–5 (2015).
51. Blinc, R. *Soft Modes in Ferroelectrics and Antiferro-electrics* (North-Holland, Amsterdam, 1974).
52. Zhang, L., Zhong, W.-L. & Kleemann, W. A study of the quantum effect in $BaTiO_3$. *Phys. Lett. A* **276**, 162–166 (2000).
53. Landau, D. P. & Binder, K. *A Guide to Monte Carlo Simulations in Statistical Physics* (Cambridge Univ. Press, Cambridge, 2014).
54. Bergqvist, L., Eriksson, O., Kudrnovskỳ, J., Drchal, Va, Korzhavyi, P. & Turek, I. Magnetic percolation in diluted magnetic semiconductors. *Phys. Rev. Lett.* **93**, 137202 (2004).